

---

# TEMPORAL CAUSAL-BASED SIMULATION FOR REALISTIC TIME-SERIES GENERATION

---

**Nikolaos Gkorgkolis\***

Department of Computer Science  
University of Crete, and  
FORTH, Heraklion, Greece  
gkorgkolis@csd.uoc.gr

**Nikolaos Kougioulis\***

Department of Computer Science  
University of Crete, and  
FORTH, Heraklion, Greece  
kougioulis@csd.uoc.gr

**MingXue Wang**

Huawei Ireland Research Centre  
Dublin, Ireland  
wangmingxue1@huawei.com

**Bora Caglayan**

Huawei Ireland Research Centre  
Dublin, Ireland  
bora.caglayan@huawei.com

**Andrea Tonon**

Huawei Ireland Research Centre  
Dublin, Ireland  
andrea.tonon1@huawei-partners.com

**Dario Simionato**

Huawei Ireland Research Centre  
Dublin, Ireland  
dario.simionato1@h-partners.com

**Ioannis Tsamardinos**

Department of Computer Science  
University of Crete, and  
FORTH, Heraklion, Greece  
tsamard@csd.uoc.gr

## ABSTRACT

Causal Discovery plays a pivotal role in revealing relationships among observed variables, particularly in the temporal setup. While the majority of CD methods rely on synthetic data for evaluation, and recently for training, these fall short in accurately mirroring real-world scenarios; an effect even more evident in temporal data. Generation techniques depending on simplified assumptions on causal structure, effects and time, limit the quality and diversity of the simulated data. In this work, we introduce *Temporal Causal-based Simulation* (TCS), a robust framework for generating realistic time-series data and their associated temporal causal graphs. The approach is structured in three phases: estimating the true lagged causal structure of the data, approximating the functional dependencies between variables and learning the noise distribution of the corresponding causal model, each part of which can be explicitly tailored based on data assumptions and characteristics. Through an extensive evaluation process, we highlight that single detection methods for generated data discrimination prove inadequate, accentuating it as a multifaceted challenge. For this, we detail a Min-max optimization phase that draws on AutoML techniques. Our contributions include a flexible, model-agnostic pipeline for generating realistic temporal causal data, a thorough evaluation setup which enhances the validity of the generated datasets and insights into the challenges posed by realistic data generation. Through experiments involving not only real but also semi-synthetic and purely synthetic datasets, we demonstrate that while sampling realistic causal data remains a complex task, our method enriches the domain of generating sensible causal-based temporal data.

---

\*Authors contributed equally to this work.

**Keywords** Causal Discovery, Causal Data Simulation, Structural Causal Models, Classifier 2-Sample Test, Generative Models, Time-series

## 1 Introduction

The field of Causal Discovery (CD) [Pearl, 2009, Spirtes et al., 2001] concerns uncovering the underlying relationships between interacting variables in observed data samples. In recent years, significant attention has shifted on unwrapping the causal structure on temporal data (i.e. time-series data) Runge [2018], Runge et al. [2019]. To evaluate the performance of CD algorithms, methods must be assessed on pairs of datasets and their ground truth causal graphs. Thus, acquiring a wide range of diverse data and causal graph pairs remains crucial. Works regarding CD algorithms on both *iid* and temporal data, tend to focus on testing either on i) *purely synthetic data* (causal models with randomized Erdős-Renyi Brouillard et al. [2020] or Barabási-Albert [Barabási and Albert, 1999] structures) or ii) *semi-synthetic data*, based on existing knowledge of real cases and scenarios (e.g., simulated Markov processes of physical systems). Examples of such datasets include the Kuramoto model of coupled oscillators [Kuramoto, 1975, Löwe et al., 2022] and brain connectivity models such as fMRI [Smith et al., 2011].

While both synthetic and semi-synthetic data are commonly used for benchmarking, they present significant shortcomings, as their resemblance to real scenarios is either unaddressed or disputable. Most of the existing causally-aware synthetic data generators are independently tailored to each research work. The vast majority implements Structural Causal Models (SCMs) [Pearl, 2009] or Vector Autoregressive Models (VARs), with randomly chosen causal assignments and functional dependencies between variables. These functional dependencies are often selected from a family of explicitly defined functions, linear and non-linear. Generated data also remain sensitive to parametric assumptions by the generator, such as predefined noise distributions.

Although some methods allow for more extensive customization and diversity during data generation Lawrence et al. [2020], they share a common denominator. The assumptions of both purely synthetic and semi-synthetic causally generated data are unlikely to hold in practice, as real-world models are subject to inherent restrictions and do not fit under closed conditions assumed by such methods. Moreover, assumptions such as the absence of latent confounders or biases in data generation, are ignorantly made without being validated in corresponding real-world scenarios. Despite these common realizations, literature works on the realistic causal generation are still almost non-existent. To our knowledge, there have been only a few, quite recent initial efforts that address the topic [Cheng et al., 2024, Cinquini et al., 2021, Wen et al., 2021], but these come under a minimal scope. Specifically, the work of Cheng et al. [2024] outputs a summary graph; this renders the method incompatible with potential applications that demand a time-wise refined structure (e.g., the training of contemporary Foundation Causal Models for CD [Stein et al., 2024]). Additionally, by adopting a restricted evaluation setup, assessments on the quality and applicability of generated data might be misleading.

In response to the aforementioned issues, we propose a generic solution on the causal-based generation of realistic time-series, that comes with a flexible implementation and a thorough evaluation pipeline. Specifically, we split the simulation process into three distinct phases: (i) the estimation of the true lagged causal structure, (ii) the approximation of the functional dependencies and (iii) the estimation of the noise distributions. The outcomes of these three phases contribute to the creation of a Temporal Structural Causal Model (TSCM), which in turn enables the generation of realistic time-series data, accompanied by their time-lagged causal structure. Each of these three phases may be approached with different methods that encapsulate the characteristics of different datasets; based on that observation, we test different methods and configurations for each phase and return the best performing causal model. Quite similar to the core of Generative Adversarial Networks (GANs) [Goodfellow et al., 2014, Goudet et al., 2017, Kalainathan et al., 2022], the final causal model is selected based on the outcome of various discriminator models, that aim to distinguish real data from simulated ones, resulting in an enriched and multifaceted evaluation process. Our main contributions can be summarized as follows:

1. We introduce a flexible, configurable and model-agnostic pipeline for generating realistic temporal causal data, based on finding the best performing causal model at each case.
2. We propose a thorough evaluation setup by optimizing the configuration of a variety of discriminator models.
3. In contrast to other initial works on the subject, we provide a more refined temporal causal structure outcome, expanding the usage of the simulated data.
4. We highlight two crucial observations about the causal generation of realistic time-series; realistic generation still poses a significant challenge, while the selection of the evaluation process can be tricky and misleading.

While the method presented in our study is capable of being applied to a variety of scenarios due to the modularity and evaluation step, the scope of our work introduces certain limitations. An important limitation is inherited from Causal

Discovery assumptions by the employed methods, such as Causal Sufficiency, as well as input and generated data being purely observational.

## 2 Related Work

There is a plethora of works in literature addressing the causal generation of synthetic data, either temporal or atemporal, but there are few to none that consider and evaluate their realistic characteristics [Cinquini et al., 2021, Wen et al., 2021]. Concerning time-series data, there are several methods considering sophisticated and configurable generative frameworks for both data and causal structure (e.g., Lawrence et al. [2020]), their approach still based on purely synthetic, randomly generated data. More precisely, although the authors allow for the inclusion of multiple target variables<sup>1</sup> (presumably for causal inference purposes), inclusion of latent confounders, configurable number of parents and children, they still implement their generation methods using Structural Causal Models and restrict the functional dependencies on collections of known functions. Such an approach, although widely used, produces data and structures with debatable realism. Methods based on generating realistic time-series data from physical systems under controlled experimental conditions have been recently introduced, such as Causal Chambers by Gamella et al. [2024]. A key difference between our approach and this work is that our pipeline is purely algorithmic instead of a closed and controlled experimental setup. The method closest to ours is CausalTime [Cheng et al., 2024], although highly different in the generation process and the qualitative outcome. The method begins by fitting a residual-based neural network (Causally Disentangled Neural Network (CDNN)), based on either an MLP or an LSTM architecture, to model a VAR process, using all historical variables for a specified maximum lag; it then extracts a hypothetical causal graph (HCG) based on computed feature importance values, using methods such as Deep Shapley Additive exPlanations (DeepSHAP) [Lundberg and Lee, 2017], while able to generate data auto-regressively. Concerning the learning process of the aforementioned work, fitting a generative model on all historical variables creates an easier problem instance compared to our proposed approach, in which we first perform CD, then fit predictive models on each variable independently, taking into account only the discovered lagged parents. As a result though, the extracted hypothetical causal graph is a *summary graph* and not a *window lagged graph* - therefore simplifying temporal causal information (i.e.  $X$  causes  $Y$  with lag  $\ell$  is lost and represented plainly as an edge  $X \rightarrow Y$  and this prohibits the use of the *CausalTime*'s outcome in applications where the causal edge's time lag is required). Finally, there are several differences between the evaluation process of *CausalTime* and our proposed method, as we optimize the used discriminators and avoid several pitfalls during the generation assessment.

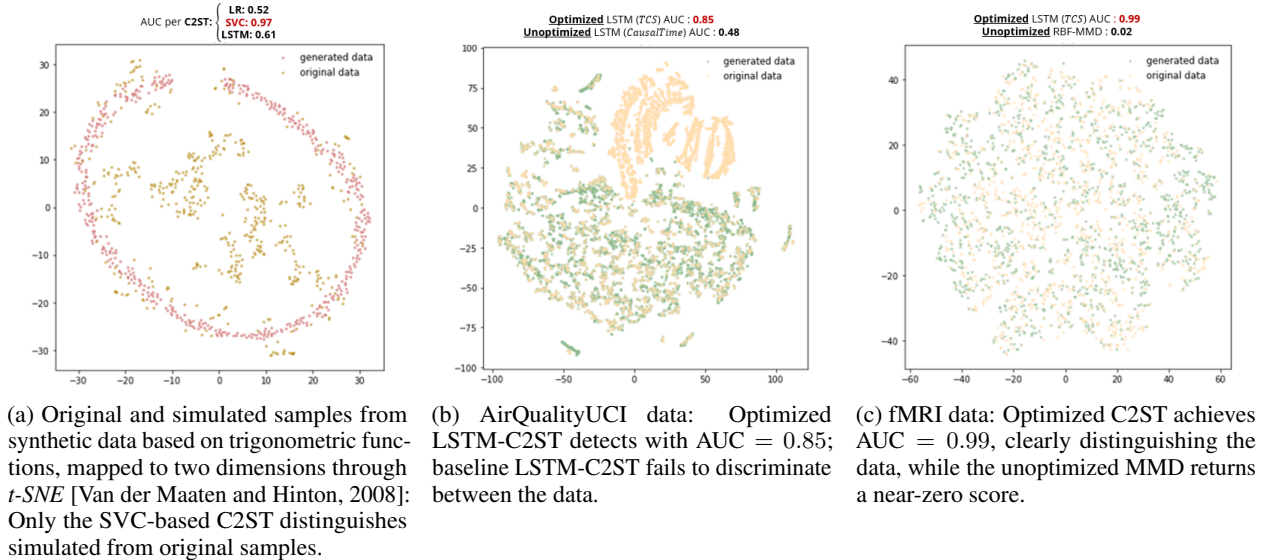


Figure 1: t-SNE projections of original and simulated data across different datasets. Optimized C2ST variants outperform standard methods (e.g., MMD) in detecting distributional differences, even when visual separability is low.

<sup>1</sup>We will be using the terms "time-series" and "variables" interchangeably when the context refers to temporal data only.

### 3 Methodology

#### 3.1 Preliminaries & Problem Formulation

In this work, our aim is to tackle the problem of *generating realistic temporal data and their corresponding causal mechanisms based on real time-series data with unknown ground truth causal graph*. We are mainly based upon the theory of Causality as introduced by Pearl [2009], i.e. Pearlian Causality, generalized to temporal data [Runge, 2018]. Consider a *temporal dataset* of  $k$  observed time-series (variables) over  $n$  time-steps, that is,  $\{\mathbf{x}_i\}_{i=1}^n$  where  $\mathbf{x} = (x^1, \dots, x^k)$  is a multivariate time-series. The backbone of modeling a causal system is the scheme in which causal relationships between variables are represented. In the Structural Causal Model (SCM) framework, the observed (endogenous) variables in the system are expressed as functions of other variables within the system and an exogenous noise term. Among others, the noise term allows to handle non-determinism in the system and acknowledge weak interactions from unobserved confounders [Peters et al., 2017]. To represent a multivariate time-series  $\mathbf{V}_t = (V_t^1, \dots, V_t^k)$  at time-step  $t$ , we follow the temporal SCM formulation of Runge [2018], by considering interactions up to a certain lag  $\ell_{\max} \in \mathbb{Z}^+$ , which is

$$V_t^j := f^j \left( \mathbf{Pa} \left( V_t^j \right), \epsilon_t^j \right), \quad \forall V_t^j \in \mathbf{V}_t, \quad t \in \mathbb{Z} \quad (1)$$

where  $\mathbf{Pa}(V_t^j) \in \{\mathbf{V}_{t-1}, \dots, \mathbf{V}_{t-\ell_{\max}}\} \setminus \{V_t^j\}$  are the *lagged causal parents* of  $V_t^j$ . The  $\coloneqq$  symbol implies *causation being asymmetric*. Although graph structures that account for unobserved confounders exist Günther et al. [2023], we model the causal graph as a Directed Acyclic Graph (DAG), where edges move towards time. An edge from  $V_{t-\tau}^i$  to  $V_t^j$  is interpreted as  $V^i$  being a *direct cause* of  $V^j$  with lag  $\tau$ , while *indirect causation* is implied through directed paths. We do not consider contemporaneous effects, that is, edges of the form  $V_t^i \rightarrow V_t^j$  between different time-series over the same time-step. This can occur when causal effects exist beyond the presumptive granularity (e.g. hourly causal mechanisms against a daily assumed lag). In our methodology, we adopt known assumptions in Causality, more specifically *Causal Markov Condition*, *Faithfulness*, *Causal Sufficiency* and *Causal Stationarity*. We refresh their definitions in Appendix A. Regarding the form of  $f$ , we consider noise to be additive,

$$f^j \left( \mathbf{Pa} \left( V_t^j \right), \epsilon_t^j \right) \equiv f^j \left( \mathbf{Pa} \left( V_t^j \right) \right) + \epsilon_t^j$$

When the causal structure and causal generative mechanism is known in Equation 1, generation of data samples from the SCM is carried out using *causal ancestral sampling*, in a similar way to ancestral sampling in Latent Variable Models (LVMs) [Murphy, 2023, Section 4.2.5]: Sample variables with no parents from a predefined noise distribution. For variables with parents, update their values based on their functional dependencies. In the temporal setting, the parent variables are fetched from the lagged parents at each timestep in the SCM, while initial values of the sampling process are being discarded (warm-up steps) to ensure stabilization in the generated data samples.

#### 3.2 Temporal Causal-based Simulation (TCS)

In this section we cover the main algorithm for generating realistic time-series data and their respective causal graph, called *Temporal Causal-based Simulation (TCS)*, depicted in Figure 2. Its main steps can be briefly described as follows:

**Phase 1: Causal Discovery** The first phase of TCS consists of the retrieval of the data's causal structure. To achieve this, we employ a variety of CD methods for time-series, which have either been established as a gold standard or express the current state-of-the-art. Specifically, we consider the algorithms *PCMCI* [Runge, 2018], *DYNOTEARS* [Pamfil et al., 2020] and *CausalPretraining* (CP) [Stein et al., 2024]. PCMCI is a CD method based on conditional independence testing, established through literature. DYNOTEARS constitutes an extension of the NOTEARS [Zheng et al., 2018] CD algorithm on temporal data, based on continuous optimization. Finally, CausalPretraining is a temporal CD neural network model, inspired by Foundation Models, that approaches the time-series CD task through end-to-end learning, trained on large amounts of synthetic instances using a decoder-only Transformer architecture. Further details on the aforementioned techniques and their hyperparameters can be found in Appendix D.2.

It is crucial to highlight that the outcome of all the considered time-series CD methods are refined lagged graphs, in contrast to similar works that focus on summary graph outputs. The trade-off here is that, while this constitutes a more challenging problem for TCS and may negatively affect the following phases, it provides an output that can be used in more applications, and can always be mapped to a summary graph, if needed.

The TCS algorithm is described in detail in Algorithm 3 of the Appendix. Given a multivariate time-series dataset  $\mathcal{D}$  over  $\mathbf{V}$ , the first phase performs temporal causal discovery using an CD algorithm dependent on a given parameter configuration  $\mathbf{B}_{\text{CD}}$  (e.g. for DYNOTEARs, the regularization constants  $\lambda_{\mathbf{W}}, \lambda_{\mathbf{A}} \in \mathbf{B}_{\text{CD}}$ ). That is, obtain:

$$\mathcal{G}, \{\mathbf{Pa}_{X^i}\}_{i \in \mathbf{V}} \leftarrow \text{causalAlg}(\mathcal{D}, \mathbf{B}_{\text{CD}}) \quad (2)$$

where  $\mathcal{G}$  is the temporal causal graph and  $\{\mathbf{Pa}_{X^i}\}_{i \in \mathbf{V}}$  notates the lagged causal parents of each time-series on the causal graph (i.e. if  $X^1$  causes  $X^2$  with a lag of 2, then in the lagged causal graph there exists an edge  $X_{t-2}^1 \rightarrow X_t^2$ , that is,  $X_{t-2}^1$  is a lagged causal parent of  $X^2$ ).

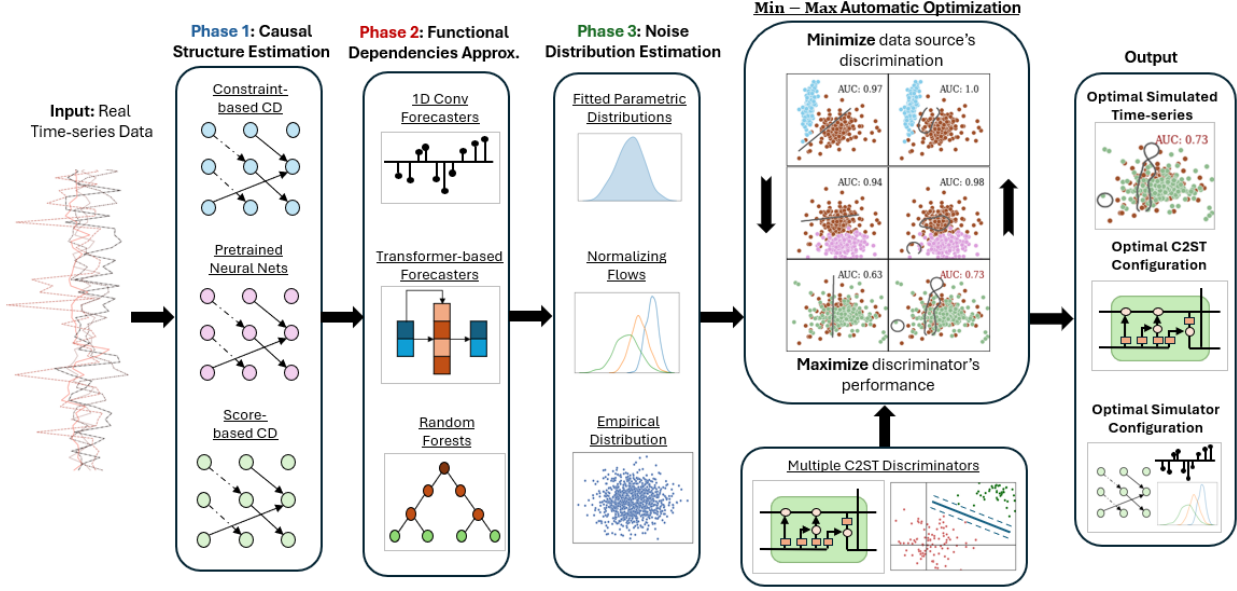


Figure 2: Illustration of *Temporal Causal-based Resimulation* (TCS). Given a multivariate time-series sample of real data, the method begins by estimating the lagged causal graph through established temporal CD methods (*phase 1*). It then estimates the functional dependencies between variables using a wide range of forecasters (*phase 2*). Based on the predictions of these forecasters, it learns the noise distribution through a variety of density estimation methods (*phase 3*). Inspired by AutoML, this process creates a set of differently configured quantitated causal models, then eventually returns the best-performing one through a Min-max optimization process, assessing against the optimal detector from a variety of C2ST methods (*Min-max optimization*).

**Phase 2: Estimation of functional Dependencies** After the causal structure of the data has been retrieved, we estimate the functional dependencies between variables by fitting forecasting methods on the past (lagged) parent values of each variable. For the time being, we incorporate three model options for the forecasting task. The first consists of classic *Random Forest* [Breiman, 2001] (RF) models on lagged data representations according to the maximum discovered time lag  $\ell_{\max}$  during the fist phase of the algorithm. The second option incorporates the *AD-DSTCN*, a 1-D Convolutional forecaster utilized by Nauta et al. [2019] in their proposed TCDF method. The last addition to our forecaster options is the recent TimesFM foundation model for time-series forecasting, introduced by Das et al. [2024]. Considering the time-series  $X^i$ , we now apply (or fit) a predictive model  $f$  on its lagged parents  $\mathbf{Pa}_{X^i}$ , to obtain an approximation of the functional dependency as in the SCM formulation. Mathematically,

$$f(X^i | \mathbf{Pa}_{X^i}) \leftarrow \text{FIT}(X^i, \mathbf{Pa}_{X^i}, \mathbf{B}_{\text{pred}}) \quad (3)$$

where FIT corresponds to the predictive algorithm used. Like in the CD phase,  $\mathbf{B}_{\text{pred}}$  is the algorithm-dependent parameter configuration. A thorough description of the implemented forecasters and their respective hyperparameters is available in Appendix D.1.

**Phase 3: Estimation of Noise Distribution** The estimation of the functional dependencies is followed by the estimation of the true noise distribution for each variable. The predictions of the fitted forecasting models are utilized to

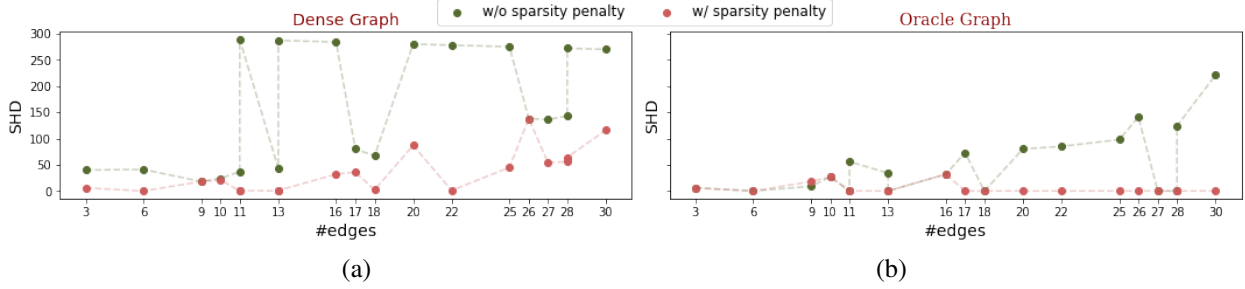


Figure 3: **(a)**: Parallel calls of TCS w/ and w/o the sparsity penalty, while providing a fully-connected lagged causal graph in the 1<sup>st</sup> phase outputs. The selected causal graphs are compared to the ground truth through SHD, where low SHD scores mean the graphs resemble each other. Calls w/ sparsity penalty successfully avoid the fully connected graph as a candidate solution. **(b)**: Parallel calls of TCS w/ and w/o the sparsity penalty, while providing ground-truth as an oracle lagged causal graph in the 1<sup>st</sup> phase outputs. Similarity measured through SHD, as in (a). In vast majority, calls with the sparsity penalty successfully chose the oracle graph as the optimal solution. This also proves the efficacy of TCS’s CD phase.

obtain the residual terms by subtracting the real data values of the corresponding time-steps. In case a variable at hand has no deduced causal parents from Phase 1, a trivial predictor is used instead, namely the mean of the true values - a solution dependent on the assumption of time-series stationarity. The result of this process corresponds to the empirical distribution of the noise, which we then utilize with several different approaches. That is, for a variable  $X_i$  and a noise configuration  $\mathbf{B}_{\text{noise}}$ , fit the noise estimator  $\epsilon_i \leftarrow \text{FIT}(\mathbf{B}_{\text{noise}})$ .

The first approach consists of fitting a Neural Flow-based model to estimate the true distribution of the noise. The models incorporated for the time being are Neural Spline Flows [Durkan et al., 2019] and a simplistic version of the RealNVP model [Dinh et al., 2017]. Details on both models and their implementation can be found in Appendix D.3. The second approach included in the framework is to assume a known parametric distribution for the noise of the data (e.g., Normal) and fit its parameters on the empirical noise distribution. The last incorporated option is to sample noise values from the empirical distribution as is.

**Min-max Optimization** Finally, we leverage on the multiple available options per phase, to create a search space  $C$  for the optimal configuration of TCS. Particularly, for each simulation, a grid search is performed on all possible combinations of components per phase; each such instance is then assessed against the original data, using the best-performing discriminator from an enriched set of detection algorithms (Section 4.2), and eventually the prevailing TCS configuration is returned. The detection algorithms are optimized on the AUC metric. To provide flexibility and keep running times manageable, the search spaces for each component are also configurable; e.g., one could adjust for a fixed forecaster (Phase 2) and noise estimator components (Phase 3) and search in between the three available CD methods (Phase 1).

## 4 Experiments and Evaluation

### 4.1 Datasets

We evaluate the performance of TCS on both real world time-series data and (semi-)synthetic data. For real-data, we adopt datasets well-used throughout the deep learning forecasting literature [Hahn et al., 2023], ranging from healthcare to finance and weather domains: The *ETTh1* and *ETTm1* data collections [Wu et al., 2021] record hourly and quarter-hourly measurements respectively of electricity transformers, as well as oil and load temperature in a two-year span between July 2016-2018. The *WTH* dataset [Jiang et al., 2023] consists of 35064 hourly atmospheric measurements, including temperature, humidity, wind speed, direction and pressure starting from January 1st 2010. The *AirQualityUCI* corresponds to 12 hourly measurements of metal oxide chemical sensors in an Italian city. The *bike-usage* dataset contains 52584 hourly wire and infrared sensor measurements of both bike and pedestrian data at the Burke–Gilman Trail in King County, Washington<sup>2</sup>, for a total of 5 time-series, while the *Outdoors* dataset contains outdoor BME280 sensor measurements from Nanning, China between February 21st 2016 and November 25th 2016, for a total of 1440 time-steps. Lastly, we include the *Air\_Quality* dataset, consisting of hourly data from 36 monitoring stations across China, as in Cheng et al. [2024].

<sup>2</sup>Data is publicly available by the City of Seattle Open Data Portal (last accessed Oct 26, 2024).

Complementary to simulating on real data, an evaluation is also being done on both semi-synthetic and purely synthetic data. The *Finance* dataset [Nauta et al., 2019] consists of simulated stationary financial portfolio data, as in Huang and Kleinberg [2015], created using the Fama-French Three-Factor Model [Fama and French, 1992]. Although the generated data are semi-synthetic and non-linear, the simulation model accounts for noise inclusion. We choose 6 datasets with 25 portfolio variables, with a total of 4000 observations. The *fMRI* collection consists of 27 datasets with 5, 10 and 15 variables and observation length from 50 to 5000. They consist of simulated BOLD (Blood-oxygen-level dependent) data, measuring the neural activity of a given brain region based on the change of blood flow (one dataset for each interest region) [Smith et al., 2011], fed through a non-linear balloon model Buxton et al. [1998]. From the above collection, we consider datasets with sample size larger than 500, which results in a selection of 6 datasets. Regarding purely synthetic data, we include a collection of datasets (*C1*) generated from non-linear Additive Noise Models, briefly described in Appendix F. More information regarding the datasets can be found in Appendix E.

Most (semi-)synthetic datasets include by default their causal structure. For several real datasets, features can be associated with their spatial coordinates, resulting in an assumed ground truth causal graph based on the Euclidean distances between the time-series (used extensively in Cheng et al. [2024]). *TCS* is also capable of considering such causal graphs (as long as they are temporal), by bypassing the CD phase. Despite that, here we opt not to include any prior knowledge, keeping uniform testing conditions in all cases (real, semi-synthetic and synthetic).

## 4.2 Metrics & Min-max Optimization

To evaluate the performance of the proposed simulation method, we need to assess whether the distribution of the simulated data  $\mathcal{P}_{\text{sim}}$  follows the distribution of the true data  $\mathcal{P}_{\text{true}}$ . Ultimately, the choice of an optimal evaluation metric for generative models remains an multifarious problem [Goudet et al., 2018]. Related works tend to employ a wide range of approaches, from basic univariate non-parametric statistical methods, such as the Kolmogorov-Smirnov 2-sample test [Pratt and Gibbons, 1981], to multivariate kernel-based solutions such as Maximum Mean Discrepancy (MMD) Gretton et al. [2012] and Classifier 2-Sample Tests (C2ST) Lopez-Paz and Oquab [2017]. In the later case, a classifier is trained to distinguish between real and generated data samples, with its test AUC score returned as the evaluation score, where a score close to 1/2 indicates indistinguishable distributions.

Concerning the use of complex parameterized evaluation methods, e.g., the detection through C2STs, we notice that the hyperparameter configuration plays an important role, especially in case of high-dimensional data with complex functional dependencies (e.g., Figure 1). In general, different metrics may prove to have independent behavior, especially in high dimensions Goudet et al. [2018].

We address this issue by leaning mainly on detection through C2STs and following two distinct phases: firstly, we enrich our evaluation pipeline with multiple classifiers; secondly, we fine-tune the hyperparameter configuration of each classifier on the given task. The classifiers that we consider for the C2ST detection are the *Support Vector Classifier* (SVC) [Hearst et al., 1998], and *Long Short-Term Memory-based Classifier* (LSTM) [Hochreiter, 1997], both optimized through hyperparameter tuning Hutter et al. [2019] to obtain the configuration that yields the best ROC-AUC score on the task.

This provides a much more systematic assessment of the generated data quality compared to evaluating on a single classifier and hyperparameter configuration. Given the lack of a universally robust 2-sample classifier, this AutoML [Hutter et al., 2019] approach consists a more adaptive and robust solution to this multifarious problem. It maps our problem formulation to a *Min-max problem* by selecting the highest discriminative score  $d \in D$  (max) obtained across the configurations  $c \in C$  of the lowest scores (min). In this criterion, we optimize with respect to the worst-case performance as  $\min_{c \in C} \max_{d \in D} d_C$ . This approach highly resembles the training process of Generative Adversarial Networks, where the data simulation algorithm resembles the generator and the Classifier 2-sample test the discriminator, and has been employed by several efforts on CD [Goudet et al., 2017, Kalainathan et al., 2022]. A high score in the above formulation assures that the generated ones remain distinguishable from the real counterparts, thus indicating shortcomings in the generative model. Conversely, a low score supports the quality of the generated samples.

Complementary to C2Ts AUC, we also report the MMD as it is frequently done in the literature. Finally, we adopt Structural Hamming Distance (*SHD*) for graph comparison during CD Efficacy.

**Sparsity Penalty** A drawback of the proposed min-max optimization is that it may occasionally favor dense graph outputs to more realistic candidate solutions of phase 1, being statistically beneficial during the next phases. To avoid this, we adopt the *sparsity penalty* from Biza et al. [2022]. Specifically, we construct a permutation-based statistical hypothesis test, on whether two classifiers have statistically equivalent scores. The permutation test is based on swapping the per sample predicted probabilities of two classifiers and then recalculating and comparing the permuted outcomes to the ground-truth; details can be seen in Algorithm 1. Through this, we find candidate TCS solutions that are statistically

---

**Algorithm 1** AUC Statistical Equivalence Test

---

**Input:** Test set labels  $y_{test}$ , discriminator predictions on the optimal configuration output  $probs_o$ , discriminator predictions on a candidate configuration output  $probs_i$ , AUC score of the optimal configuration output against the true data  $AUC_o$ , AUC score of a candidate configuration output against the true data  $AUC_i$ , significance level  $a$ , number of permutations  $n$

**Output:** *True* or *False* for statistical equivalence

```
tobs ← |AUCo – AUCi|
ctr ← 0
for  $p = 1$  to  $n$  do
|  $w_l^p$  := random prediction indices to swap
|  $probs_w^o, probs_w^i \leftarrow \text{swap}(probs_o, probs_i, w_l^p)$ 
|  $AUC_o^w \leftarrow \text{evaluate}(y_{test}, probs_w^o)$ 
|  $AUC_i^w \leftarrow \text{evaluate}(y_{test}, probs_w^i)$ 
|  $t_p \leftarrow |AUC_o^w - AUC_i^w|$ 
| if  $t_p > t_{obs}$  then
| | ctr ← ctr + 1
|
end
pvalue ←  $\frac{ctr}{n}$ 
if  $pvalue \geq a$  then
| Return True
|
else
| Return False
|
end
```

---

equivalent to the best-performing one. We then filter through all candidate solutions by choosing the one with the sparsest causal graph. The efficacy of the sparsity penalty is tested under two different validating experiments and displayed at Figure 3. Both experiments are performed on synthetic data generated through non-linear additive noise models (Appendix F), with Gaussian noise and the same number of nodes (10), but with an increasing edge density per graph, ranging from 3 to 30. The results highlight the necessity for the sparsity penalty and validate its usefulness.

## 4.3 Results

### 4.3.1 Comparison to Current State-of-the-Art

To evaluate the performance of the proposed methodology, *TCS* is applied on a varying collection of datasets, including real, semi-synthetic and synthetic data, as described in Section 4.1. As none of the considered methods account for non-stationary time-series, each time-series stationarity has been fact-checked through the Augmented Dickey-Fuller [Dickey and Fuller, 1979] unit root test (Appendix B). For collections of datasets, the mean scores are obtained, along with their standard errors. For single datasets, we sample representative sequences of 2000 samples per dataset, similarly to Block Bootstrap [Gonçalves and Politis, 2011, Härdle et al., 2003]. Sampling is repeated 10 times per dataset. To provide a comparison with the current state-of-the-art, the recent *CausalTime* method is also employed, strictly following the implementation details provided by the authors<sup>3</sup>. For a fair comparison, we also adopt the preprocessing scheme of *CausalTime*, where potential missing values are imputed through interpolation. The results of the comparison are depicted in Table 1 for real, synthetic and semi-synthetic time-series.

### 4.3.2 CD Efficacy

To further evaluate *TCS*, we test the CD efficacy of the simulated datasets. In detail, we adapt the common ML Efficacy test on the CD task, by using the original and simulated data as the subject of the CD method, and compare the similarity of the two outputs based on their AUC. A high AUC score means that the simulated data act similar to the original. The CD method used is DYNOTEARs, with the configuration  $\ell_{max} = 1$ ,  $\lambda_w = 0.1$  and  $\lambda_a = 0.1$ . We did not optimize on its configuration, as the goal of the experiment is to test the similarity of the output rather than the accuracy of the CD method; nonetheless, other time-series CD methods were also tested, which yielded similar behavior. For the sake of comparison, both *CausalTime* and our proposed methodology were incorporated; the results are reported in Table 2.

<sup>3</sup>The GitHub codebase of *CausalTime* is publicly available here.

Table 1: Comparison on Real and Semi-Synthetic Data. Both *TCS* and *CausalTime* are evaluated using the proposed optimized C2ST metric (AUC) and a non-optimized MMD score. On real data, both methods struggle to simulate distributions indistinguishable from the original, with MMD often diverging from classifier performance. On semi-synthetic data, simulations show more promise—especially for TCS on fMRI and C1 datasets—though performance still varies across datasets. This supports our main conclusions: causal simulation of time-series remains challenging, and non-optimized metrics can be misleading.

| Dataset       | MMD                               |                                   | AUC                               |                                   |
|---------------|-----------------------------------|-----------------------------------|-----------------------------------|-----------------------------------|
|               | TCS                               | CausalTime                        | TCS                               | CausalTime                        |
| AirQuality    | $1.30 \pm 0.74$                   | <b><math>0.32 \pm 0.01</math></b> | $0.97 \pm 0.00$                   | <b><math>0.84 \pm 0.00</math></b> |
| AirQualityUCI | <b><math>0.46 \pm 0.02</math></b> | $1.12 \pm 0.04$                   | $0.99 \pm 0.00$                   | <b><math>0.83 \pm 0.00</math></b> |
| ETTh1         | <b><math>0.75 \pm 0.16</math></b> | $1.53 \pm 0.12$                   | $0.92 \pm 0.02$                   | <b><math>0.80 \pm 0.00</math></b> |
| ETTm1         | <b><math>0.27 \pm 0.02</math></b> | $1.47 \pm 0.04$                   | $0.93 \pm 0.00$                   | <b><math>0.82 \pm 0.00</math></b> |
| Bike-usage    | <b><math>0.23 \pm 0.02</math></b> | $0.38 \pm 0.01$                   | $0.88 \pm 0.01$                   | <b><math>0.77 \pm 0.00</math></b> |
| Outdoors      | $2.36 \pm 0.00$                   | <b><math>2.20 \pm 0.00</math></b> | $0.99 \pm 0.00$                   | <b><math>0.83 \pm 0.00</math></b> |
| WTH           | <b><math>0.28 \pm 0.07</math></b> | $0.69 \pm 0.02$                   | $0.85 \pm 0.01$                   | <b><math>0.80 \pm 0.00</math></b> |
| fMRI          | <b><math>0.08 \pm 0.01</math></b> | $0.77 \pm 0.10$                   | <b><math>0.71 \pm 0.01</math></b> | $0.78 \pm 0.01$                   |
| Finance       | <b><math>0.26 \pm 0.02</math></b> | $1.02 \pm 0.02$                   | $0.99 \pm 0.00$                   | <b><math>0.78 \pm 0.00</math></b> |
| C1            | <b><math>0.09 \pm 0.11</math></b> | $0.90 \pm 0.02$                   | <b><math>0.57 \pm 0.00</math></b> | $0.77 \pm 0.00$                   |

Table 2: CD Efficacy: AUCs of the causal graphs derived from simulated data against the ground truth. A high AUC score indicates the simulated data act similar to the original on CD tasks. Both methodologies display similar performance. *fMRI*, *C1*, *Finance*, and *AirQuality* favor **TCS**, while *AirQualityUCI*, *ETTh1*, *ETTm1*, and *Outdoors* favor CausalTime. The results suggest that simulated time-series from both methods capture enough characteristics of the original data distribution for CD methods to behave comparably.

| Dataset       | Method      |             |
|---------------|-------------|-------------|
|               | TCS         | CausalTime  |
| AirQuality    | <b>0.86</b> | 0.77        |
| AirQualityUCI | 0.73        | <b>0.99</b> |
| ETTh1         | 0.63        | <b>0.99</b> |
| ETTm1         | 0.70        | <b>0.98</b> |
| Bike Usage    | 0.73        | 0.73        |
| Outdoors      | 0.67        | <b>0.99</b> |
| WTH           | 0.99        | 0.99        |
| fMRI          | <b>0.95</b> | 0.93        |
| Finance       | <b>0.99</b> | 0.74        |
| C1            | <b>0.76</b> | 0.65        |

### 4.3.3 Temporal Causal-based vs Conventional Simulation

To further validate of the proposed pipeline, we provide a comparison between causally simulated and non-causally simulated samples. In the second case, no causal relationships between time-series are taken into account during the generation phase, and data simulation is performed by conventional temporal generative models. The examples provided in Table 3 are generated using i) *CPAR* [Zhang et al., 2022], a conditional probabilistic auto-regressive generative model, as implemented by *SDV* [Patki et al., 2016] and ii) *TimeVAE* [Desai et al., 2021], a variational autoencoder model, available through the *Synthcity* [Qian et al., 2023] framework. We use the proposed evaluation setup and the same datasets to maintain clarity. We expect non-causal simulation approaches to achieve better performance, as they deal with a less perplexed problem. The obtained results, though, display close performance for all considered methods, which raises the competitiveness of the non-conventional, causal-based simulators in general. We note that the presented experiment is quite limited to be considered representative, and more cases of non-causal simulators and dataset should be considered in later efforts.

Table 3: Benchmarks against non-causal simulation: *TCS* and *CausalTime* are compared against the non-causal probabilistic generative models *CPAR* and *TimeVAE* on time-series simulation. We assume non-causal models to be advantageous, as they do not depend on finding a causal graph. Nonetheless, all considered methods perform comparably (AUC $\sim 0.85$  on real, AUC $\sim 0.75$  on synthetic), with few exceptions favoring *TCS* and *CausalTime*.

| Dataset       | Method                 |                         |                 |                        |
|---------------|------------------------|-------------------------|-----------------|------------------------|
|               | TCS                    | CausalTime              | CPAR            | TimeVAE                |
| WTH           | 0.85 $\pm 0.01$        | <b>0.80</b> $\pm 0.00$  | 0.99 $\pm 0.00$ | 0.98 $\pm 0.00$        |
| AirQualityUCI | 0.99 $\pm 0.01$        | <b>0.83</b> $\pm 0.00$  | 0.99 $\pm 0.00$ | 0.95 $\pm 0.00$        |
| AirQuality    | 0.97 $\pm 0.00$        | <b>0.84</b> $\pm 0.00$  | 0.98 $\pm 0.00$ | 0.99 $\pm 0.00$        |
| ETTh1         | 0.92 $\pm 0.00$        | <b>0.80</b> $\pm 0.00$  | 0.95 $\pm 0.00$ | 0.91 $\pm 0.00$        |
| ETTm1         | 0.93 $\pm 0.00$        | <b>0.82</b> $\pm 0.00$  | 0.96 $\pm 0.00$ | 0.91 $\pm 0.00$        |
| Bike Usage    | 0.88 $\pm 0.01$        | <b>0.77</b> $\pm 0.00$  | 0.90 $\pm 0.00$ | 0.83 $\pm 0.00$        |
| Outdoors      | 0.99 $\pm 0.00$        | 0.83 $\pm 0.00$         | 0.99 $\pm 0.00$ | <b>0.81</b> $\pm 0.00$ |
| fMRI          | <b>0.71</b> $\pm 0.01$ | 0.78 $\pm 0.01$         | 0.74 $\pm 0.02$ | 0.75 $\pm 0.00$        |
| Finance       | 0.99 $\pm 0.00$        | <b>0.78</b> $\pm 0.000$ | 0.99 $\pm 0.00$ | 0.86 $\pm 0.00$        |
| C1            | <b>0.57</b> $\pm 0.00$ | 0.77 $\pm 0.00$         | 0.63 $\pm 0.01$ | 0.81 $\pm 0.00$        |

## 5 Conclusion, Discussion & Future Work

In this paper, we proposed *Temporal Causal-based Simulation*, a method for generating realistic temporal data and their corresponding causal graph, by leveraging real-world time-series data. *TCS* approaches simulation through 3 distinct phases; each phase investigates a variety of techniques, from established CD methods to neural normalizing flows and large pre-trained models, to discover the best performing causal model each time. To achieve this, it leverages multiple C2STs as discriminators, through an AutoML Min-max optimization scheme that compares the quantitated causal models against the optimal discriminator. We also expand the benchmark datasets of similar previous efforts, including numerous real datasets and several synthetic and semi-synthetic collections. *TCS* is thoroughly assessed against causal and non-causal state-of-the art simulators, with our experiments revealing two main outcomes: the first is that realistic causal generation of temporal data, unlike the claims of other works, remains an unsolved problem; the second is that the use of optimized evaluation processes is necessary. Nonetheless, we show *TCS*’s successful performance on synthetic data and competitiveness on real cases, while its modular design allows it to benefit as causal algorithms improve. We believe that the presented pipeline significantly contributes to the Causal Discovery domain, as algorithms can now be evaluated on richer and more diverse data representations compared to their synthetic counterparts. Realistic causal data simulation could also prove beneficial for temporal Causal Foundation Models [Stein et al., 2024], which tend to be depended solely on restrictive synthetic data. While our method shows promising results, limitations exist that provide avenues for further research. As future work, we aim to expand the broader capabilities of the method by including more robust flow models such as Glow [Kingma and Dhariwal, 2018], further enhance the Min-max optimization phase with flexible AutoML techniques such as Bayesian Optimization [Hutter et al., 2019] and account for non-stationarity.

## 6 Reproducibility Statement

The complete source code, including documentation, implementation and benchmarking scripts, is publicly available at <https://github.com/gkorgkolis/TCS>.

## Acknowledgements

We would publicly like to thank Konstantina Biza and Étienne Vareille for their fruitful comments throughout this work.

## References

- Albert-László Barabási and Réka Albert. Emergence of scaling in random networks. *Science*, 286(5439), 1999.
- Konstantina Biza, Ioannis Tsamardinos, and Sofia Triantafillou. Out-of-sample tuning for causal discovery. *IEEE Transactions on Neural Networks and Learning Systems*, 35(4), 2022.

- Leo Breiman. Random forests. *Machine Learning*, 45, 2001.
- Peter J Brockwell and Richard A Davis. *Time series: Theory and Methods*. Springer, 1986.
- Philippe Brouillard, Sébastien Lachapelle, Alexandre Lacoste, Simon Lacoste-Julien, and Alexandre Drouin. Differentiable causal discovery from interventional data. *Advances in Neural Information Processing Systems*, 2020.
- Richard B Buxton, Eric C Wong, and Lawrence R Frank. Dynamics of blood flow and oxygenation changes during brain activation: the balloon model. *Magnetic Resonance in Medicine*, 39(6), 1998.
- Yuxiao Cheng, Ziqian Wang, Tingxiong Xiao, Qin Zhong, Jinli Suo, and Kunlun He. Causaltime: Realistically generated time-series for benchmarking of causal discovery. In *International Conference on Learning Representations*, 2024.
- Martina Cinquini, Fosca Giannotti, and Riccardo Guidotti. Boosting synthetic data generation with effective nonlinear causal discovery. In *IEEE CogMI*. IEEE, 2021.
- Abhimanyu Das, Weihao Kong, Rajat Sen, and Yichen Zhou. A decoder-only foundation model for time-series forecasting. *arXiv preprint arXiv:2310.10688*, 2024.
- Abhyuday Desai, Cynthia Freeman, Zuhui Wang, and Ian Beaver. Timevae: A variational autoencoder for multivariate time series generation. *arXiv preprint arXiv:2111.08095*, 2021.
- David A Dickey and Wayne A Fuller. Distribution of the estimators for autoregressive time series with a unit root. *Journal of the American Statistical Association*, 74(366a), 1979.
- Laurent Dinh, Jascha Sohl-Dickstein, and Samy Bengio. Density estimation using RealNVP. *International Conference on Learning Representations*, 2017.
- Conor Durkan, Artur Bekasov, Iain Murray, and George Papamakarios. Neural spline flows. *Advances in Neural Information Processing Systems*, 2019.
- Eugene F Fama and Kenneth R French. The cross-section of expected stock returns. *The Journal of Finance*, 47(2), 1992.
- Juan L Gamella, Jonas Peters, and Peter Bühlmann. The causal chambers: Real physical systems as a testbed for ai methodology. *arXiv preprint arXiv:2404.11341*, 2024.
- Tomas Geffner, Javier Antoran, Adam Foster, Wenbo Gong, Chao Ma, Emre Kiciman, Amit Sharma, Angus Lamb, Martin Kukla, Nick Pawlowski, et al. Deep end-to-end causal inference. *Transactions of Machine Learning Research*, 2024.
- Silvia Gonçalves and Dimitris Politis. Discussion: Bootstrap methods for dependent data: A review. *Journal of the Korean Statistical Society*, 40(4), 2011.
- Ian Goodfellow, Jean Pouget-Abadie, Mehdi Mirza, Bing Xu, David Warde-Farley, Sherjil Ozair, Aaron Courville, and Yoshua Bengio. Generative adversarial networks. In *Advances in Neural Information Processing Systems*, 2014.
- Olivier Goudet, Diviyan Kalainathan, Philippe Caillou, Isabelle Guyon, David Lopez-Paz, and Michèle Sebag. Causal generative neural networks. *arXiv preprint arXiv:1711.08936*, 2017.
- Olivier Goudet, Diviyan Kalainathan, Philippe Caillou, Isabelle Guyon, David Lopez-Paz, and Michele Sebag. Learning functional causal models with generative neural networks. *Explainable and Interpretable Models in Computer Vision and Machine Learning*, 2018.
- Arthur Gretton, Karsten Borgwardt, Malte Rasch, Bernhard Schölkopf, and Alex Smola. A kernel method for the two-sample-problem. *Advances in Neural Information Processing Systems*, 2006.
- Arthur Gretton, Karsten M Borgwardt, Malte J Rasch, Bernhard Schölkopf, and Alexander Smola. A kernel two-sample test. *Journal of Machine Learning Research*, 13, 2012.
- Wiebke Günther, Urmi Ninad, and Jakob Runge. Causal discovery for time series from multiple datasets with latent contexts. In *Uncertainty in Artificial Intelligence*. PMLR, 2023.
- Yannik Hahn, Tristan Langer, Richard Meyes, and Tobias Meisen. Time series dataset survey for forecasting with deep learning. *Forecasting*, 5(1), 2023.
- Wolfgang Härdle, Joel Horowitz, and Jens-Peter Kreiss. Bootstrap methods for time series. *International Statistical Review*, 71(2), 2003.
- M.A. Hearst, S.T. Dumais, E. Osuna, J. Platt, and B. Schölkopf. Support vector machines. *IEEE Intelligent Systems and their Applications*, 13(4), 1998.
- S Hochreiter. Long short-term memory. *Neural Computation*, 1997.
- Yuxiao Huang and Samantha Kleinberg. Fast and accurate causal inference from time series data. In *The Twenty-Eighth International Flairs Conference*, 2015.

- Frank Hutter, Lars Kotthoff, and Joaquin Vanschoren. *Automated Machine Learning: aMethods, Systems, Challenges*. Springer Nature, 2019.
- Maowei Jiang, Pengyu Zeng, Kai Wang, Huan Liu, Wenbo Chen, and Haoran Liu. Fecam: Frequency enhanced channel attention mechanism for time series forecasting. *Advanced Engineering Informatics*, 58, 2023.
- Diviyan Kalainathan, Olivier Goudet, Isabelle Guyon, David Lopez-Paz, and Michèle Sebag. Structural agnostic modeling: Adversarial learning of causal graphs. *Journal of Machine Learning Research*, 23(219), 2022.
- Durk P Kingma and Prafulla Dhariwal. Glow: Generative flow with invertible 1x1 convolutions. *Advances in Neural Information Processing Systems*, 2018.
- Yoshiki Kuramoto. Self-entrainment of a population of coupled non-linear oscillators. In *International Symposium on Mathematical Problems in Theoretical Physics: Kyoto University, Kyoto/Japan*. Springer, 1975.
- Andrew R. Lawrence, Marcus Kaiser, Rui Sampaio, and Maksim Sipos. Data generating process to evaluate causal discovery techniques for time series data. *NeurIPS Causal Discovery & Causality-Inspired Machine Learning Workshop*, 2020.
- David Lopez-Paz and Maxime Oquab. Revisiting classifier two-sample tests. In *International Conference on Learning Representations*, 2017.
- Sindy Löwe, David Madras, Richard Zemel, and Max Welling. Amortized causal discovery: Learning to infer causal graphs from time-series data. In *CLeaR*. PMLR, 2022.
- Scott M Lundberg and Su-In Lee. A unified approach to interpreting model predictions. *Advances in Neural Information Processing Systems*, 2017.
- Kevin P Murphy. *Probabilistic Machine Learning: Advanced Topics*. MIT Press, 2023.
- Meike Nauta, Doina Bucur, and Christin Seifert. Causal discovery with attention-based convolutional neural networks. *Machine Learning and Knowledge Extraction*, 1(1), 2019.
- Roxana Pamfil, Nisara Sriwattanaworachai, Shaan Desai, Philip Pilgerstorfer, Konstantinos Georgatzis, Paul Beaumont, and Bryon Aragam. DYNOTEARS: Structure learning from time-series data. In *AISTATS*. PMLR, 2020.
- George Papamakarios, Eric Nalisnick, Danilo Jimenez Rezende, Shakir Mohamed, and Balaji Lakshminarayanan. Normalizing flows for probabilistic modeling and inference. *Journal of Machine Learning Research*, 22(57), 2021.
- Neha Patki, Roy Wedge, and Kalyan Veeramachaneni. The synthetic data vault. In *IEEE DSAA*. IEEE, 2016.
- Judea Pearl. *Causality*. Cambridge University Press, 2nd edition, 2009.
- Jonas Peters, Dominik Janzing, and Bernhard Schölkopf. *Elements of Causal Inference: Foundations and Learning Algorithms*. MIT Press, 2017.
- John Winsor Pratt and Jean Dickinson Gibbons. *Concepts of Nonparametric Theory*. Springer, 1981.
- Zhaozhi Qian, Bogdan-Constantin Cebere, and Mihaela van der Schaar. Synthcity: Facilitating innovative use cases of synthetic data in different data modalities, 2023. URL <https://arxiv.org/abs/2301.07573>.
- Danilo Rezende and Shakir Mohamed. Variational inference with normalizing flows. In *International Conference on Machine Learning*. PMLR, 2015.
- Jakob Runge. Causal network reconstruction from time series: From theoretical assumptions to practical estimation. *Chaos: An Interdisciplinary Journal of Nonlinear Science*, 28(7), 2018.
- Jakob Runge, Sebastian Bathiany, Erik Bollt, Gustau Camps-Valls, Dim Coumou, Ethan Deyle, Clark Glymour, Marlene Kretschmer, Miguel D Mahecha, Jordi Muñoz-Marí, et al. Inferring causation from time series in earth system sciences. *Nature Communications*, 10(1), 2019.
- Jakob Runge, Andreas Gerhardus, Gherardo Varando, Veronika Eyring, and Gustau Camps-Valls. Causal inference for time series. *Nature Reviews Earth & Environment*, 4(7), 2023.
- Stephen M Smith, Karla L Miller, Gholamreza Salimi-Khorshidi, Matthew Webster, Christian F Beckmann, Thomas E Nichols, Joseph D Ramsey, and Mark W Woolrich. Network modelling methods for fmri. *Neuroimage*, 54(2), 2011.
- Peter Spirtes, Clark Glymour, and Richard Scheines. *Causation, Prediction, and Search*. MIT Press, 2001.
- Gideon Stein, Maha Shadaydeh, and Joachim Denzler. Embracing the black box: Heading towards foundation models for causal discovery from time series data. *AAAI AI4TS Workshop*, 2024.
- Laurens Van der Maaten and Geoffrey Hinton. Visualizing data using t-sne. *Journal of Machine Learning Research*, 9 (11), 2008.

- Bingyang Wen, Luis Oliveros Colon, KP Subbalakshmi, and Rajarathnam Chandramouli. Causal-tgan: Generating tabular data using causal generative adversarial networks. *arXiv preprint arXiv:2104.10680*, 2021.
- Haixu Wu, Jiehui Xu, Jianmin Wang, and Mingsheng Long. Autoformer: Decomposition transformers with auto-correlation for long-term series forecasting. *Advances in Neural Information Processing Systems*, 2021.
- Kevin Zhang, Neha Patki, and Kalyan Veeramachaneni. Sequential models in the synthetic data vault. *arXiv preprint arXiv:2207.14406*, 2022.
- Xun Zheng, Bryon Aragam, Pradeep K Ravikumar, and Eric P Xing. Dags with NOTEARS: Continuous optimization for structure learning. *Advances in Neural Information Processing Systems*, 2018.
- Haoyi Zhou, Shanghang Zhang, Jieqi Peng, Shuai Zhang, Jianxin Li, Hui Xiong, and Wancai Zhang. Informer: Beyond efficient transformer for long sequence time-series forecasting. *AAAI*, 2021.

## A Causal Assumptions

All Causal Discovery algorithms are governed by a set of assumptions, regarding the statistical properties of the data and the underlined structure of the causal model. The following assumptions are defined in a way to be applied to either a (standard) causal graph or a temporal causal graph.

**Definition 1** (Causal Markov Condition, [Spirtes et al., 2001]). *Let  $\mathcal{G}$  be a causal graph with vertex set  $\mathbf{V}$  and  $\mathbb{P}$  a probability distribution over  $\mathbf{V}$ , generated by the causal structure induced by  $\mathcal{G}$ . Then  $\mathcal{G}$  and  $\mathbb{P}$  satisfy the Markov Condition if and only if  $\forall W \in \mathbf{V}, W$  is independent of its non-descendants (non causal effects) given its parents (direct causes) on  $\mathcal{G}$ .*

**Definition 2** (Faithfulness, [Spirtes et al., 2001]). *Let  $\mathcal{G}$  be a causal graph and  $\mathbb{P}$  a probability distribution over  $\mathbf{V}$ . We say that  $\mathcal{G}$  and  $\mathbb{P}$  are faithful to each other if and only if the all and only the independence relations of  $\mathbb{P}$  are entailed by the Causal Markov condition of  $\mathcal{G}$ . Specifically,  $\mathcal{G}$  and  $\mathbb{P}$  satisfy the Faithfulness Condition if-f every conditional independence relation true in  $\mathbb{P}$  is entailed by the Causal Markov Condition applied to  $\mathcal{G}$ .*

**Definition 3** (Causal Sufficiency, [Spirtes et al., 2001]). *A set  $\mathbf{V}$  of variables is causally sufficient for a population if and only if in the population every common cause of any two or more variables in  $\mathbf{V}$  is in  $\mathbf{V}$ , or has the same value for all units in the population. The common cause  $Z$  of two or more variables in a DAG  $X \leftarrow Z \rightarrow Y$  is called a confounder of  $X$  and  $Y$ . Hence Causal Sufficiency implies no unobserved confounders. The notion of causal sufficiency is being used without explicitly mentioning the population.*

**Definition 4** (Causal Stationarity, [Runge, 2018]). *Consider the SCM description in Equation 1. If the causal relationships between variables  $(V_{t-\tau}^i, V_t^j)$  for time lag  $\tau > 0$  also hold for all time-shifted versions  $(V_{t'-\tau}^i, V_{t'}^j)$ , the described process is causally stationary. Informally, the graph structure and noise distribution of the SCM does not change over time.*

**Definition 5** (Time-series Stationarity, [Brockwell and Davis, 1986]). *Let  $\{X_t\}_{t \in \mathbb{Z}}$  be a time-series with index set  $\mathbb{Z} = \{0, \pm 1, \pm 2, \dots\}$ . The series is said to be stationary if:*

1.  $\mathbb{E}|X_t|^2 < \infty, \quad \forall t \in \mathbb{Z}$
2.  $\mathbb{E}X_t = m, \quad \forall t \in \mathbb{Z}$
3.  $\gamma_X(r, s) = \gamma_X(r + t, s + t), \quad \forall r, s, t \in \mathbb{Z}$

where  $\gamma_X(r, s) = \mathbb{E}[(X_r - \mathbb{E}X_r)(X_s - \mathbb{E}X_s)]$ ,  $r, s \in \mathbb{Z}$  is the autocovariance function of the stochastic process  $\{X_t\}_{t \in \mathbb{Z}}$ .

## B Dickey-Fuller Test

Consider the AR(1) model  $Y_t = \alpha Y_{t-1} + X_t$ ,  $t = 1, 2, \dots$  where  $\{X_t\}$  is a stationary process, the process  $Y_t$  is *non-stationary* if  $\alpha = 1$  and *stationary* if  $|\alpha| < 1$ . The test is based on the empirical value of the t-statistic derived from a simple regression of the form  $\Delta Y_t = Y_t - Y_{t-1} = (\alpha - 1)Y_{t-1} + \epsilon_t$  where  $\Delta Y_t$  represents the first difference of the time-series. With the Dickey-Fuller Dickey and Fuller [1979] test, one checks the null hypothesis  $H_0 : \alpha - 1 = 0$  (indicating the presence of a unit root) against  $H_1 : \alpha - 1 \neq 0$ . The t-statistic is calculated as  $t = \hat{\beta}/s_{\hat{\beta}}$  where  $\hat{\beta} = \hat{\alpha} - 1$  is the estimated coefficient and  $s_{\hat{\beta}}$  its standard error. If the calculated t-value is less than the critical value given by the Dickey-Fuller distribution table, statistical significance is observed; otherwise, we accept that there is a unit root making the time-series non-stationary.

The Augmented Dickey-Fuller test expands the Dickey-Fuller test in order to include higher order lagged terms of the differenced time-series to the autoregressive process.

## C Experimental Details

Experiments have been run on a dedicated workstation with a single Nvidia RTX 4090 24GB GPU, 128GB physical RAM and implemented in PyTorch. We have also opted to implement some metrics in Tensorflow to ensure consistency in the experimental results.

## D Implemented CD Algorithms, Forecasters & Noise Estimators

An overview of the implemented methods for CD, functional dependency and noise estimation is illustrated in Table 4.

Table 4: Implemented Methods for Temporal Functional Dependency Estimation, Noise Density Estimation, and Temporal Causal Discovery.

| Temporal Causal Discovery               |   |
|---|---|
| Method                                  | Description                                 |
| PCMCI [Runge, 2018]                     | Constraint-Based Algorithm                  |
| DYNOTEARS [Pamfil et al., 2020]         | Constraint Optimization Algorithm           |
| CP [Stein et al., 2024]                 | Pre-trained Transformer                     |
| Functional Dependency Estimation        |   |
| Random Forest Regressor [Breiman, 2001] | Ensemble Learning Regressor                 |
| AD-DSTCN [Nauta et al., 2019]           | Time-series Forecasting Model (TCDF module) |
| TimesFM [Das et al., 2024]              | Foundational Time-series Forecaster         |
| Noise Density Estimation                |   |
| Normal Distribution                     | Fitted Parametric Distribution              |
| Uniform Distribution                    | Fitted Parametric Distribution              |
| Neural Splines [Durkan et al., 2019]    | Normalizing Flows                           |
| RealNVP [Dinh et al., 2017]             | Normalizing Flows                           |

## D.1 Predictive Methods

### D.1.1 AD-DSTCN

AD-DSTCN stands for *Attention-based Dilated Depth-wise Separable Temporal Convolutional Networks* and it constitutes a time-series forecasting model, based on a 1D convolutional neural network, derived from the time-series causal discovery methodology *TCDF* [Nauta et al., 2019].

In its original definitions, AD-DSTCN consists of multiple forecasting neural networks  $N_j$ , where each network corresponds to a variable  $j$  in the input data. All networks  $N_j$  are *1D convolutional* and implement a so called *causal convolution*, in the sense that during training, the model predicts the time-series value for the next time-step while being restricted to only the previous time-steps values, avoiding any information leakage in time. The *depth-wise separable* characteristic refers to the use of separate kernel filters per input channel, in contrast to the common practice of using the same kernel for all channels. This is commonly known as *depth-wise convolution*, and it is a key modification that aids AD-DSTCN to attend multivariate time-series instead of univariate ones. Dilation is also incorporated, as a mean to increase the receptive field of the model (i.e., the number of time steps captured by the kernel filter). Dilation in convolutions is performed through the application of the kernel filter on areas larger than its size, which in turn is achieved by skipping input values by a predefined step size hyperparameter. Residual connections are also added in each channel after each convolution, from the input of the convolution to the output, but with the first layer excluded. Finally, AD-DSTCN has a learnable attention layer added up-front based on multiplicative attention, that attends on all the input univariate time-series, as a way to indicate which variate contributes more in each prediction. The computed attention scores are highly related with the causal discovery framework TCDF, as they are interpreted accordingly to find causal relations for each target univariate time-series in the data.

For the implementation of the model, we choose the following parameters empirically, achieving a satisfactory trade-off between model complexity and performance, illustrated in Table 5.

Table 5: AD-DSTCN Architecture hyperparameters.

| Parameter                                  | Value  |
|--|--------|
| Training epochs                            | $10^3$ |
| Dilation coefficient $c_{\text{dilation}}$ | 2      |
| Learning rate (lr)                         | 0.01   |
| Kernel size ( $k$ )                        | 2      |
| Hidden layer blocks                        | 0      |

### D.1.2 Random Forest Regressors

Random Forests [Breiman, 2001] belong to the family of ensemble learning methods that combine multiple decision trees to improve predictive accuracy and control overfitting, compared to individual decision trees, mitigating disadvantages like high variance and sensitivity to noise in the data. In our study, we implement the regressor with the `sklearn.ensemble` module. The Random Forest Regressor is configured with 1000 tree estimators ensure prediction robustness, no imposed tree-depth limits, use of all available features for each split as well as bootstrap resampling.

### D.1.3 TimesFM

TimesFM [Das et al., 2024] is a foundation model for time-series forecasting, trained on a versatile corpus of 100 billion time-points. The architecture utilizes a decoder-only Transformer model with multiple causal self-attention (also referred to as masked self-attention) layers, while key features of the model include patches, where contiguous time-points are treated as tokens, as well as the ability to handle variable-length inputs and different forecasting horizons.

We utilize the `timesfm-1.0-200m-pytorch` model, with 200M parameter size, with a training checkpoint available from the authors at HuggingFace. Regarding the selection of parameters, we opt for the default ones suggested by the authors. More specifically, an input patch length of 32, 512 context length (which must be a multiple of patch size), an output patch length of 128, 128 horizon length 20 decoder layers and model dimension  $d_{\text{model}} = 1280$ .

## D.2 Causal Discovery Methods

### D.2.1 PCMCI

Peter-Clark Momentary Conditional Independence (PCMCI) is a time-series causal discovery algorithm introduced by Runge [2018]. It is based on the constraint-based Peter-Clark (PC) algorithm by Spirtes et al. [2001], uncovering causal relationships using conditional independence tests of the form  $X_i(t - \tau) \rightarrow X_j(t)$  for lag  $\tau = 0, \dots, \ell_{\max}$ . The algorithm assumes the causal Markov condition, faithfulness causal stationarity and causal sufficiency and also accounts for contemporaneous ( $\tau = 0$ ) causation. The process consists of two phases, i) the PC phase where it prunes spurious relationships by testing if a variable is conditionally independent of another variable, given a conditioning set and ii) the MCI phase where, using Momentary Conditional Independence, it tests for causal relationships while conditioning on both lagged and contemporaneous variables.

In our implementations we use the official implementation of PCMCI, available in the `Tigramite` Python package. We select  $\alpha = 0.05$  as the threshold of the adjacency matrix's p-values exclude contemporaneous edges,  $\ell_{\max} = 1$ . For independence tests we utilize partial correlation, which is estimated through a linear Ordinary Least Squares (OLS) regression and testing for non-zero linear Pearson correlation on the residuals and GPDC, which is a conditional independence test based on Gaussian processes and distance correlation.

### D.2.2 DYNOTEARs

DYNOTEARs [Pamfil et al., 2020] is a time-series causal discovery algorithm, viewed as an extension of the the NOTEARS [Zheng et al., 2018] method, which introduced causal discovery as a mathematical optimization problem with smooth acyclicity constraint. By leveraging the trace exponential function to enforce acyclicity and promoting sparsity using the  $\ell_1$  norm, this optimization program is solved using the augmented Lagrangian method, translating it into a series of unconstrained problems, in a similar setup to NOTEARS. Assuming  $M$  independent realizations of a *stationary* time-series  $\{x_{m,t}\}_{t=0}^T$  for  $\mathbf{x}_{m,t} \in \mathbb{R}^d$ , the authors model the data using a Linear Structural Vector Autoregression (SVAR) model. Assuming causal stationarity (Appendix A), the model is expressed as

$$\mathbf{x}_{m,t} = \mathbf{x}_{m,t}W + \sum_{i=1}^p \mathbf{x}_{m,t-i}A_i + \mathbf{z}_{m,t},$$

where  $W$  represents contemporaneous (*intra-slice*) dependencies,  $A_i$  lagged (*inter-slice*) dependencies, and  $\mathbf{z}_{m,t}$  independent error terms. In matrix form,

$$\mathbf{X} = \mathbf{X}W + \mathbf{Y}A + \mathbf{Z},$$

where  $\mathbf{X}$  contains the observations,  $\mathbf{Y}$  the time-lagged versions of  $\mathbf{X}$  and  $A$  is the concatenated matrix of lagged weights. The parameters of DYNOTEARs, apart from  $\ell_{\max}$ , are the regularization constants  $\lambda_W$ ,  $\lambda_A$  that control

the sparsity (as causal graphs are in general sparse), and the weight thresholds  $\tau_{\mathbf{W}}$ ,  $\tau_{\mathbf{A}}$  that reduce the numerical error when computing  $h(\mathbf{W} = \text{trace}(e^{\mathbf{W} \circ \mathbf{W}}) - d$ . In our implementations, we select  $\lambda_{\mathbf{W}} = \lambda_{\mathbf{A}} = 0.1$ , thresholds  $\tau_{\mathbf{W}} = \tau_{\mathbf{A}} = 0.05$ , maximum number of iterations in the augmented Lagrangian method  $n = 100$  and  $\ell_{\max} = 1$ . Since DYNOTEARS' formulation is based on intra-slice and inter-slice dependencies for modeling the influence between variables in a contemporaneous and time-lagged setting respectively, we drop the contemporaneous predictions as we assume no contemporaneous effects in our experimental setup.

### D.2.3 Causal Pretraining

Causal Pretraining Stein et al. [2024] is a causal discovery method for time-series data inspired by Foundation Models. The authors introduce (but not limited to) a decoder-only Transformer architecture similar to the Informer [Zhou et al., 2021] time-series forecaster (but without ProbSparse Attention) and a modified final layer adapted for predicting a lagged adjacency tensor. Similar to PCMC, the maximum number of lags  $\ell_{\max}$  is considered as a hyperparameter of the model. The method assumes causal sufficiency and causal stationarity, as well as no contemporaneous effects and an assumption on the existence of a single causal edge between two variables, called *one-lag per cause*. A disadvantage of the method is the limiting training and input size of the pre-trained model: The authors provide pre-trained models on purely synthetic data (temporal data and ground truth causal graph) up to 5 variables and 3 lags, which limits causal discovery on larger datasets. Additionally, the input size, which in this case refers to the maximum number of samples to be considered - time-series length, is constrained to 500. Moreover, the authors argue that extending the architecture and training the model for higher number of variables and lags significantly lowers predictive performance.

Table 6: Architecture details for our custom trained CP model, as described in Appendix D.2.3. Model dimension is denoted as  $d_{\text{model}}$ .

| Parameter                           | Value         |
|-------------------------------------|---------------|
| Epochs                              | $10^3$        |
| Patience                            | 10            |
| Learning Rate                       | $10^{-3}$     |
| $d_{\text{model}}$                  | 512           |
| Num. of Attention Heads             | 8             |
| Encoder Layers                      | 4             |
| Feed-Forward Dimension              | 2048          |
| Dropout Rate                        | 0.05          |
| Max Time-series Length              | 500           |
| Attention Distillation              | True          |
| <b>Num. of Trainable Parameters</b> | <b>17.1 M</b> |

In order to alleviate this issue and extend our pipeline with a pre-trained model that enables much faster inference compared to constraint-based causal discovery methods, we train an extended version of the model, on 100K synthetic data pairs, containing samples up to 12 variables and 3 lags. The above have been generated in accordance to Appendix F. As the input of the Informer architecture is fixed, we apply, as in Stein et al. [2024], normal noise padding to the samples and zero padding to the lagged adjacency tensor for data less than 12 variables and 3 lags. It must be noted that training the CP model on data derived from our synthetic data generator results in a much more robust model and higher predictive performance than the ones argued by the authors. The authors also concatenate the empirical autocorrelation of the samples to the model input during the training as well as the inference phase, called *correlation injection*, which we find successfully aids the model to confidently include/exclude edges with high/low autocorrelation respectively. In this work, we make use of the *deep* architecture, which we re-train and adapt as described previously. We argue that this choice of model parameters provides a fine balance between model performance, parameter size and weight sharability. The details of the architecture are shown in Table D.2.3. Since the model is trained with data containing up to 12 time-series, its usage is excluded from the pipeline for multivariate time-series input of size higher than 12.

## D.3 Density Estimation Methods

**Normalizing Flows** Normalizing flows [Rezende and Mohamed, 2015, Papamakarios et al., 2021] represent a class of generative models that enable tractable estimation of densities by transforming a simple initial distribution into a complex one with a series of bijective (differentiable and invertible) mappings, using the change of variables formula. As such, mappings are chosen to have an exact and tractable computation of the Jacobian determinant.

### D.3.1 RealNVP

RealNVP [Dinh et al., 2017] serves as an extension of the Nonlinear Independent Components Estimation (NICE) model. Similar to NICE, it consists of coupling and rescaling layers. The input sample  $\mathbf{x} \in \mathbb{R}^d$  is split into  $\mathbf{x} \equiv (\mathbf{x}_1, \mathbf{x}_2)$ , being transformed into  $\mathbf{y}_1 = \mathbf{x}_1$  and  $\mathbf{y}_2 = \mathbf{x}_2 \circ \exp(s(\mathbf{x}_1)) + t(\mathbf{x}_1)$  where  $s(\cdot)$ ,  $t(\cdot)$  are the rescaling and translation functions (typically, MLPs). The inverse transform is  $\mathbf{x}_1 = \mathbf{y}_1$ ,  $\mathbf{x}_2 = \mathbf{y}_2 - t(\mathbf{y}_1) \circ \exp(-s(\mathbf{y}_1))$ . Hence, for the given transformation  $\mathbf{y} = f(\mathbf{x})$ , the density  $p_X(\mathbf{X})$  is  $p_X(\mathbf{x} = p_Y(f(\mathbf{x}))) \left| \det \frac{\partial f(\mathbf{x})}{\partial \mathbf{x}} \right|^{-1}$  with  $\log \left| \det \frac{\partial f(\mathbf{x})}{\partial \mathbf{x}} \right| = \sum_{i=1}^{d_2} s_i(\mathbf{x}_1)$  where  $d_2 = \dim(\mathbf{x}_2)$  and  $s_i(\mathbf{x}_1)$  =  $i$ -th component of  $s(\mathbf{x}_1)$ .

### D.3.2 Neural Spline Flows

Neural Spline flows [Durkan et al., 2019] extend the normalizing flows model using piecewise rational splines which allow for more expressive non-linear transformations while maintaining invertibility and computational efficiency. Neural Spline Flows have already found use in causal discovery, particularly on observational data, in the Deep End-to-End Causal Inference (DECI) [Geffner et al., 2024] model for additive noise estimation. We make use of the `Pyro` library for the implementation of splines with linear order polynomials, with 16 bins and the Adam Optimizer with a learning rate of 0.01.

## D.4 Evaluation Metrics

### D.4.1 Maximum Mean Discrepancy (MMD)

Similarity between real and synthetic data can be quantified using the *Maximum Mean Discrepancy (MMD)* [Gretton et al., 2006] metric. MMD measures the distance between two probability distributions by embedding the data into a reproducing kernel inner-product space and calculating the difference in the mean embeddings. The MMD score is given by

$$\text{MMD}^2(X, Y) = \mathbb{E}_{X, X}[k(X, X)] + \mathbb{E}_{Y, Y}[k(Y, Y)] - 2\mathbb{E}_{X, Y}[k(X, Y)]$$

where  $X$  and  $Y$  are the real and synthetic data samples respectively and the expectations are taken over all points in the selected data batch. In our experiments, we utilize the *Gaussian kernel*, defined by  $k(x, y) = \exp\left(-\frac{\|x-y\|^2}{2\sigma^2}\right)$  where, like before,  $x$  and  $y$  represent data points and  $\sigma$  the bandwidth of the kernel. We utilize a range of bandwidth multipliers, specifically  $[0.01, 0.1, 1, 10, 100]$ , in order to capture different scales of variation in our data.

### D.4.2 Classifier 2-sample tests

A fundamental problem in statistics is determining whether two samples,  $S_1 \sim P$  and  $S_2 \sim Q$ , are drawn from the same distribution. Over time, a plethora of statistical tests have been introduced. These range from parametric tests, like Student's t-test, which assume a specific form of the distribution, to non-parametric tests, such as the Kolmogorov-Smirnov test, which make no explicit distributional assumptions. All statistical tests construct a *test statistic* based on summary statistics, in order to either accept (formally, fail to reject) the null hypothesis  $H_0 : P = Q$ , or reject it.

The central idea of *Classifier 2-sample tests*, introduced by Gretton et al. [2012], is to train a machine learning classifier to distinguish data sampled from distribution  $P$  against data sampled from distribution  $Q$ . Intuitively, if the null hypothesis  $H_0 : P = Q$  holds, then the classifier should be unable to distinguish between the samples and should perform at an accuracy close to 1/2, or chance level. As Lopez-Paz and Oquab [2017] demonstrated, classifier 2-sample tests offer several attractive properties for evaluating data similarity, such as assessing the quality of samples generated by models where the likelihood is intractable but the sampling from the generating process is tractable.

**Logistic Regression (LR) Detection** The Logistic Regression (LR) Detection method utilizes a logistic regression model to distinguish between real and synthetic data samples. We utilize the `SDMetrics` implementation from the Synthetic Data Vault (SDV) package, where real and synthetic datasets are merged into a single table with an additional indicator label (real vs generated). We measure the classification performance using the Area Under the ROC Curve (ROC-AUC).

**Support Vector Classifier (SVC) detection** In a similar manner to the LR 2-sample classifier, we leverage the `scikit-learn` SVC implementation. Like before, our SVC detection function merges the real and synthetic datasets in a single table and an indicator variable.

**Long Short-Term Memory (LSTM) detection** The model architecture of the Long Short-Term Memory [Hochreiter, 1997] classifier includes an LSTM layer, a fully connected layer, and a sigmoid activation for binary classification, trained with the Adam optimizer and Binary Cross Entropy as the loss function. Like before, real and generated data are merged with the model trained on a 75 % random subset of the joint data.

### D.4.3 Min-max Optimization

Table 7: Search Space Configurations for 2-sample Classifier Tests Optimization. For SVM Detection, `poly` refers to the polynomial kernel and `rbf` to Radial Basis Function.

| Detection Method | Hyperparameter  | Values                 |
|------------------|-----------------|------------------------|
| SVM Detection    | C               | {1.0, 0.75, 0.5, 0.25} |
|                  | Kernel          | {linear, poly, rbf}    |
|                  | Degree          | {3}                    |
|                  | Gamma           | {auto, scale}          |
| LSTM Detection   | Batch Size      | {32, 64}               |
|                  | Hidden Size     | {128, 256}             |
|                  | Num Layers      | {2}                    |
|                  | Dropout         | {0.1}                  |
|                  | Sequence Length | {10, 20}               |
|                  | Num Epochs      | {10}                   |
|                  | Learning Rate   | {0.0001, 0.001}        |

We deduce the 2-sample classifier testing problem to a Min-max selection problem as follows: Define a set of classifiers  $D$ , each with a set of configurations  $C_d = \{c_{d,1}, c_{d,2}, \dots, c_{d,n}\}$ . For each classifier  $d \in D$  and configuration  $c \in C_d$ , we compute the discriminative score  $d_c$  of the classifier. From these configurations, select the maximum discriminative score obtained across the set of lowest scores, that is, optimize with Min-max selection as

$$\min_{c \in C} \max_{d \in D} d_c$$

The maximization step can be interpreted as "*For each configuration  $c$ , obtain the highest discriminative score across the classifiers*", while the minimization step as "*Among all configurations, select the configuration with the lowest maximum score, which depicts the least discriminative, yet optimal case*".

For tuning, a simple grid search is employed across the configurable search spaces shown in Figure 7 that result in 1, 24 and 16 configurations for the logistic, support vector and LSTM classifiers respectively.

## E Datasets

Additionally to Section 4.1, in Tables 8 and 9 we provide a summary of the real and synthetic datasets used throughout our experiments respectively, while Table 10 shows an overview of considered semi-synthetic datasets.

## F Synthetic Data Generation

In a similar way to the synthetic temporal data - causal graph generators in `Tigramite` [Runge et al., 2023] and Stein et al. [2024], we implement our own version of a temporal SCM-based time-series generator for purely synthetic samples. Concerning noise formulation, both multiplicative and additive noise model formulation are implemented, based on Equation 1. For our experimental setup, we opted for additive noise generated data. The generation is based on the following distinct steps: Initially, the lagged temporal graph is generated, following a random DAG generation paradigm such as the Erdős-Rényi [Brouillard et al., 2020] or the Barabási-Albert [Barabási and Albert, 1999] scale-free model. Analogously to Lawrence et al. [2020], extensive configurations allow the generation of diverse purely synthetic data collections, such as the number of variables and samples, minimum and maximum lags  $\ell_{\min}, \ell_{\max}$  respectively and edge existence probability to name a few. A plethora of functional dependencies are included, ranging from linear to non-linear. Examples are linear, power and exponential, sigmoid, ReLU and trigonometric. Regarding noise distributions, normal and uniform distributions are accounted. The flexibility to include any noise distributions is also provided. In the second phase, temporal ancestral sampling [Murphy, 2023, Section 4.2.5] is performed on each node in the created lagged causal graph to obtain the generated samples. For stability purposes, warmup is included, as in Runge et al. [2023], where initial samples are discarded. The process is identical to Algorithm 2.

Table 8: Overview of Real Time-Series Datasets.

| Dataset       | Variables | Timesteps | Granularity | Start Date | Domain         |
|---------------|-----------|-----------|-------------|------------|----------------|
| ETTh1         | 7         | 17420     | 1 hour      | 07/01/2016 | Power          |
| ETTm1         | 7         | 69680     | 15 min      | 07/01/2016 | Power          |
| WTH           | 12        | 35064     | 1 hour      | 01/01/2020 | Weather        |
| Air_Quality   | 36        | 8760      | 1 hour      | -          | Weather        |
| AirQualityUCI | 12        | 9357      | 1 hour      | 03/10/2024 | Weather        |
| Bike-usage    | 5         | 552584    | 1 hour      | 01/01/2014 | Transportation |
| Outdoors      | 3         | 1440      | 1 sec       | 21/02/2016 | Environmental  |

Table 9: Overview of the Synthetic Time-Series Dataset Collection.

| Collection | Num. of Datasets | Variables | Timesteps | Max Lag | Functional Relationships |
|------------|------------------|-----------|-----------|---------|--------------------------|
| C1         | 10               | 3-12      | 1000      | 1-3     | Linear & Non-linear      |

Table 10: Overview of Semi-synthetic Time-Series Dataset Collections.

| Collection | Num. of Datasets | Variables | Timesteps   | Max Lag | Functional Relationships |
|------------|------------------|-----------|-------------|---------|--------------------------|
| fMRI       | 6                | 5         | 1200 - 5000 | 1       | Non-linear               |
| Finance    | 5                | 25        | 4000        | 1       | Non-linear               |

The way different synthetic data generation methods account for non-stationarity of the generated time-series should also be taken into account. The synthetic temporal data generator available in `Tigramite` checks for network stability using eigenvalue testing on the stability matrix, while the data generated in Stein et al. [2024], which are then used to train the neural model, are not guaranteed to be stationary. The first approach halts the data generation, rather than attempting any resampling or adjustment of the process parameters to enforce stationarity, while in the second it is tackled purely by resampling until stationarity is observed.

In our own generation process, we address this by wrapping outcomes with bounded functions, such as the hyperbolic tangent  $\tanh$  or the sigmoid function  $\sigma$ . In this way, it is ensured that applying saturating functions cap the growth of unbounded functions that lead to non-stationarity. As an additional advantage, causal dependencies are not altered and any causal relationship to the lagged adjacency matrix is preserved, hence increasing stability of the generation process and safeguarding causal stationarity. Further and extensive details on the above implementations can be found in our public GitHub repository, as shared in Section 6, where extensive documentation is provided.

## G Pseudocodes

In this section, we provided pseudocodes for TCS. Algorithm 2 describes the ancestral sampling process in a temporal SCM while 3 represents the general pipeline of the TCS method. Algorithm 4 represents the permutation-based test for the Sparsity Penalty.

---

**Algorithm 2** Temporal SCM Ancestral Sampling (ANCESTRAL)

---

**Input:** Temporal Causal Graph  $\mathcal{G}$  of time-series  $\{\mathbf{X}_t\}_{t=1}^{\ell_{\max}}$ , causal discovery algorithm configuration  $\mathbf{B}_{\text{CD}}$ , predictive model configuration  $\mathbf{B}_{\text{pred}}$ , noise estimator configuration  $\mathbf{B}_{\text{noise}}$ , max lag  $\ell_{\max} \in \mathbf{B}_{\text{CD}}$ , number of timesteps  $T$ , number of warmup steps  $W$

**Output:** Generated time-series sample  $\{\mathbf{X}_t\}_{t=1}^T$

**Initialize**  $X_{t=0}^i$  for all  $i \in \{1, \dots, N\}$  with random noise

// Forward Sampling

**for**  $t = W + \ell_{\max} + 1$  **to**  $T$  **do**

**for** each variable  $X_t^i$  in topological order based on  $\mathcal{G}$  **do**

        Determine lagged parents  $\text{Pa}_{X_t^i} \leftarrow \{X_{t-k}^j \mid (X^j, X^i) \in \mathcal{G}, 1 \leq k \leq \ell_{\max}\}$  ; // Lagged parents  $X^j$  of  $X^i$  at time  $t$

        Compute  $X_t^i := f_i(\text{Pa}_t^i) + \epsilon_t^i$

**end**

**end**

**Return** generated time-series dataset  $\{\mathbf{X}_t^i\}_{W+\ell_{\max}}^T$

---



---

**Algorithm 3** Temporal Causal-Based Simulation (TCS)

---

**Input:** Real time-series dataset  $\mathcal{D} = \{\mathbf{X}_i\}_{i=1}^T$  over time-series set  $\mathbf{V}$ , sample size  $n$ , causal discovery algorithm configuration  $\mathbf{B}_{\text{CD}}$ , predictive model configuration  $\mathbf{B}_{\text{pred}}$  and noise estimator configuration  $\mathbf{B}_{\text{noise}}$

**Output:** Simulated temporal dataset  $\mathcal{D}'$

$\mathcal{D}' \leftarrow \emptyset$

// Graph Estimation Phase

$\mathcal{G}, \mathbf{Pa} \leftarrow \text{causalAlg}(\mathcal{D}, \mathbf{B}_{\text{CD}})$ ; // Obtain temporal causal graph  $\mathcal{G}$  and lagged parents  $\mathbf{Pa}$

// Simulation Phase

**for** each variable  $X^i \in \mathcal{D}$  **do**

    // Predictive Modeling Phase

**if**  $\mathbf{Pa}_{X^i} \neq \emptyset$  **then**

        Estimate  $f(X^i \mid \mathbf{Pa}_{X^i}) \leftarrow \text{FIT}(X^i, \mathbf{Pa}_{X^i}, \mathbf{B}_{\text{pred}})$

        Compute residuals  $R_{X^i} \leftarrow X^i - f(X^i \mid \mathbf{Pa}_{X^i})$

**end**

**else**

        Compute residuals  $R_{X^i} \leftarrow X^i - \mathbb{E}[X^i]$

**end**

    // Noise Modeling Phase

    Fit noise estimator  $\epsilon^i \leftarrow \text{FIT}(\mathbf{B}_{\text{noise}})$

// Ancestral Sampling Phase

Generate time-series samples  $\{X_t^i\}_{t=1}^n$  with

$\text{ANCESTRAL}(\mathcal{G}, T, W, \ell_{\max}, \mathbf{B}_{\text{CD}}, \mathbf{B}_{\text{pred}}, \mathbf{B}_{\text{noise}})$

    Update  $\mathcal{D}' \leftarrow \mathcal{D}' \cup \{X_t^i\}$

**end**

**Return** simulated dataset  $\mathcal{D}'$ .

---

---

**Algorithm 4** AUC Statistical Equivalence Test

---

**Input:** Test set labels  $y_{test}$ , discriminator predictions on the optimal configuration output  $probs_o$ , discriminator predictions on a candidate configuration output  $probs_i$ , AUC score of the optimal configuration output against the true data  $AUC_o$ , AUC score of a candidate configuration output against the true data  $AUC_i$ , significance level  $a$ , number of permutations  $n$

**Output:** *True* or *False* for statistical equivalence

```
 $t_{obs} \leftarrow |AUC_o - AUC_i|$ 
 $ctr \leftarrow 0$ 
for  $p = 1$  to  $n$  do
   $w_l^p :=$  random prediction indices to swap
   $probs_w^o, probs_w^i \leftarrow \text{swap}(probs_o, probs_i, w_l^p)$ 
   $AUC_o^w \leftarrow \text{evaluate}(y_{test}, probs_o^w)$ 
   $AUC_i^w \leftarrow \text{evaluate}(y_{test}, probs_i^w)$ 
   $t_p \leftarrow |AUC_o^w - AUC_i^w|;$ 
  if  $t_p > t_{obs}$  then
     $ctr \leftarrow ctr + 1$ 
end

$pvalue \leftarrow \frac{ctr}{n}$

if  $pvalue \geq a$  then
  Return True
else
  Return False
end
```

---